ORIGINAL ARTICLE

Selective Transport of Airborne Microparticles Through Micro-channels Under Microgravity

Monia Makhoul[1] · Philippe Beltrame[1] (ORCID)

Abstract

This paper analyzes the possibility of obtaining the selective transport of microparticles suspended in air in a microgravity environment through modulated channels without net displacement of air. Using numerical simulation and bifurcation analysis tools, we show the existence of intermittent particle drift under the Stokes assumption of the fluid flow. The particle transport can be selective and the direction of transport is controlled only by the kind of pumping used. The selective transport is interpreted as a deterministic ratchet effect due to spatial variations in the flow and the particle drag. This ratchet phenomenon could be applied to the selective transport of metal particles during the short duration of microgravity experiments.

Keywords Transport · Ratchet effect · Microfluidic · Bifurcations · Microgravity

Introduction

Under microgravity, it is crucial to filter microparticles because the particles do not settle on the ground. In particular, any metal-cutting operation on the ISS would involve the dangerous diffusion of iron filings. Processes based on microfiltration using a membrane raise two problems, however. Firstly, they require a constant air flux; secondly, at high permeation rates, the accumulation of non-permeating particles above the membrane surface blocks the pores and rapidly decreases the filtration efficiency (Kulrattanarak et al. 2008).

In the terrestrial conditions, neither the sedimentation nor transport due to the Soret effect (Cherepanov and Smorodin 2018) allow a selective transport. In contrast, microdevices in which the membrane is replaced by

periodic microstructures through which the particles move freely induce specific trajectories of particles depending on their characteristics (density, size, etc...). In Loutherback et al. (2009), the authors showed that a particle selection is possible using an oscillating flow, i.e. without net displacement of the fluid. The particle transport occurs through a periodic structure of triangular columns. Within a certain particle size range, the lift force acts asymmetrically during the back and forth cycle of the fluid flow. This results in a drift that is orthogonal to the oscillating flow for a parameter range. The main drawback of the use of the lift force is that the particle flux is proportional to the thin width of the micro-structure since the flow is transverse.

To date, the literature has focused almost exclusively on the lift effect. The present paper, in contrast, focuses on longitudinal transport, i.e. the drift takes place along the axis of fluid oscillations. We consider a micro-device similar to Matthias and Müller (2003) and Vlasova et al. (2020) where two basins are connected via modulated channels filled with a liquid. A periodic pumping confers a back and forth fluid motion dragging the particles in suspension. For oscillating Stokes flow, the 1D transport of particles is usually explained by the Stokes drift (Santamaria et al. 2013). The drift is due to a nonzero average of the traveling wave motion along a Lagrangian trajectory. In our context, such a Lagrangian trajectory does not exist, the flow therefore needs to be ratchet like. The 'ratchet effect' refers to the possibility of transporting particles even if the mean

✉ Philippe Beltrame
philippe.beltrame@univ-avignon.fr

Monia Makhoul
mounia.makhoul@univ-avignon.fr

[1] UMR1114 EMMAH, Avignon Université – INRAE, F-84914 Avignon, France

force is zero (zero bias). In the early 2000s, the transport of overdamped particles in ratchets in many fields in physics was interpreted as a Brownian motor in which transport results from the action of noise in an asymmetric potential (Reimann 2002; Hänggi and Marchesoni 2009). Such a drift ratchet phenomenon may occur in the microfluidic context considered here (Kettner et al. 2000) and the experiment in (Matthias and Müller 2003) appeared to corroborate this theory. Nevertheless, further experiments (see Mathwig et al. (2011)) revealed that the experiment in (Matthias and Müller 2003) does not evidence transport due to a Brownian ratchet or to a deterministic ratchet.

Recently, we highlighted different 1D transport mechanisms in a Stokes flow, called *ratchet flow*, for a simple model of inertial particle. This model could be especially relevant for metal particles in air because the particle inertia is not negligible compared to fluctuations, contrary to the case of microparticles in suspension in a liquid (Matthias and Müller 2003). Moreover, under microgravity, the particle weight does not break the ratchet effect.

According to Makhoul et al. (2015a), particle transport occurs for particle sizes that are not negligible compared to the channel radius. Therefore, the drag coefficient depends on the channel walls and hence on the particle position. Such a variation may induce a friction ratchet (Luchsinger 2000; Reimann 2002).

The main goal of this paper was to determine whether such longitudinal transport mechanisms as in (Beltrame et al. 2016) exist in a micro-gravity environment for metal particles in suspension in the air. To answer this question, we consider a simplified model in which the particle is constrained to move along the channel axis and the fluid inertia is neglected (Section "Modeling"). In this framework, the particle trajectory is the solution of a nonlinear ODE system (Section "Modeling"). In Sections "Transition to Transport" and "Domain of Intermittent Drift", bifurcation analysis tools and continuation of periodic orbit provide a comprehensive overview of the dynamics in the phase space and we determine the transport domains in the parameter space. Finally, we discuss the validity of the assumptions,

especially the quasi-static approximation (Section "Domain of Validity of the Assumptions"). We show that the existence domain can be relevant for the transport of metal particles in air during micro-gravity experiments.

Modeling

Let us consider an L-periodically modulated channel infinitely extended along the line (Ox) through which a Newtonian fluid with the viscosity μ is T-periodically pumped. We call 'pore' the channel portion of length L (Fig. 1). We assume that the flow is a quasi-static and isovolume Stokes flow. The consistency of these approximations with the parameter domains of the transport solution is discussed in Section "Domain of Validity of the Assumptions". Without particles, the quasi-static velocity field $\vec{V}_0(\vec{R}, t)$ at the position $\vec{R}$ and time t reads $\vec{V}_0(\vec{R}, t) = \vec{U}_0(\vec{R})A(t)$, where $A(t)$ is the pumping amplitude at time t and $\vec{U}_0(\vec{R})$ is a stationary velocity field of periodicity L in x-direction (Kettner et al. 2000; Beltrame et al. 2016). Because of the L-periodicity, the pressure difference, noted $[p]$, between the pore inlet and outlet is constant. In the Stokes approximation, the difference $[p]$ is the pressure difference between the basins divided by the number of pores. Thereafter, we employ the dimensionless variables and equations by scaling the space, the time and the pressure by L, T and $[p]$, respectively. From now on, t refers to the dimensionless time. We denote by $\vec{r}$ the dimensionless vector position, by p^* the dimensionless pressure and by $\vec{u}_0$ the dimensionless velocity associated to $\vec{U}_0$. Then, $\vec{u}_0$ verifies the dimensionless Stokes equation:

$$\Delta \vec{u}_0(\vec{r}) = \mathcal{P}_v \nabla p^*(\vec{r}) \tag{1}$$

$$\nabla . \vec{u}_0(\vec{r}) = 0 \tag{2}$$

where $\mathcal{P}_v = \dfrac{[p]T}{\mu} \tag{3}$

with no-slip boundary conditions at the pore-wall. Even if a non negligible slip velocity is expected for a gas flow in a microchannel (Qin et al. 2007), we show in Section Domain

Fig. 1 Sketch of the problem: a spherical particle translates along the x-axis of a periodic distribution of pores. It is dragged by the periodic motion of a viscous fluid
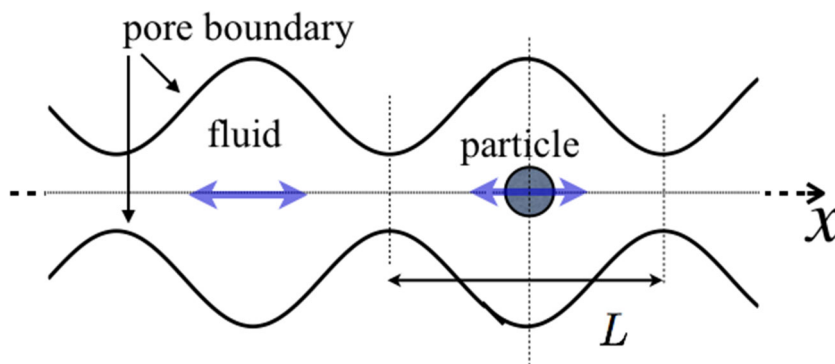
of Validity of the Assumptions that the no-slip assumption implies only an error of only a few percent on the drag force.

We consider the axisymmetric problem where the particle of mass m in suspension in the fluid moves only along the axis. A consequence of assuming the axisymmetric problem is that the particle moves along the x axis and it does not rotate. Then, the particle is entirely determined by its center position $x(t)$. Let us note $\dot{x}(t)$ and $\ddot{x}(t)$ the velocity and acceleration, respectively. The resulting drag on the particle is along the channel axis. We denote R_x the x dimensionless component of the drag. According to the scaling, the drag force is proportional to the adimensional parameter

$$\mathcal{P}_\gamma = \frac{LT\mu}{m}. \tag{4}$$

Moreover, R_x is only due to the perturbed flow and it depends linearly on the boundary condition because of the linearity of the Stokes Eq. 1. Thus, it is possible to decompose the drag force as the sum of two contributions (Makhoul et al. 2015b): $R_x = F_p + F_r$. The first contribution F_p corresponds to the drag force on a moving particle in a fluid at rest while the second term F_r is the drag force on a particle at rest in a moving fluid. F_p is proportional to the particle velocity $-\gamma(x)\dot{x}$ where $\gamma(x) > 0$ corresponds to the drag coefficient. Once $\gamma(x)$ computed, we introduce the velocity u_{eq} called *equivalent velocity*, such that $F_r = (\mathcal{P}_\gamma \gamma(x))u_{eq}(x)$ when $\mathcal{P}_v = 1$ and $A(t) = 1$. Because of the linearity of the Stokes equation, $F_r = \mathcal{P}_\gamma \gamma(x)u_{eq}(x)\mathcal{P}_v A(t)$ in the general case for arbitrary values of $\mathcal{P}_v$ and $A(t)$. Hence the drag force is written

$$R_x = \mathcal{P}_\gamma \gamma(x)\left[-\dot{x} + \mathcal{P}_v u_{eq}(x)A(t)\right] \tag{5}$$

In the limiting case of a point particle in an infinite medium $u_{eq}(x) = u_0(x)$, $\gamma(x) = \gamma_0$ is the Stokes friction and Eq. 5 is Stokes' law. For the general case of a fluid confined in a micropore with a non negligible particle size, u_{eq} depends on the pore boundary and the particle shape (Brenner 1964; Makhoul et al. 2015a). Using a Boundary Element approach, we computed the fields $u_{eq}(x)$ and $\gamma(x)$ (Makhoul et al. 2015a, b, Makhoul 2016). Note that the functions $u_{eq}(x)$ and $\gamma(x)$ are 1-periodic like the geometry of the problem. According to Newton's second law, the governing dimensionless equation of the particle position $x(t)$ is written

$$\ddot{x} + \mathcal{P}_\gamma \gamma(x)\dot{x} = \mathcal{P}_\gamma \mathcal{P}_v \gamma(x)u_{eq}(x)A(t), \tag{6}$$

We recognize a damped oscillator equation with forcing. The forcing on the right-hand side corresponds to a standing wave so it differs from the Stokes drift. If both functions are constant, then the problem is linear and only harmonic oscillations are expected. As soon as the channel radius is modulated, the functions $\gamma(x)$ and $u_{eq}(x)$ are variable and Eq. 6 is non-linear. This equation differs from Eq. 4

of Beltrame et al. (2016) by the fields $\gamma(x)$ and $u_{eq}(x)$. Both fields were given without any relation with pore shape, especially γ was assumed constant, contrary to the present study.

The pore shape is given by a sinusoidal function:

$$r(x) = r_m\left(1 + c_r \cos(2\pi x)\right) \tag{7}$$

where r_m is the mean radius and $0 < c_r < 1$ is called the *channel camber*. Then the pore shape is symmetric and the functions $u_{eq}(x)$ and $\gamma(x)$ have parity-symmetry. If, in addition, the pumping $A(t)$ varies sinusoidally, then the problem is invariant by the parity symmetry $x \to -x$. More precisely, if $x(t)$ is a trajectory given by Eq. 6 then $-x(t + 1/2)$ is also the solution for a symmetric initial condition. In order to break the parity-symmetry, the back and forth phases of the pumping should be different, i.e. this means that $A(t + 1/2) \neq -A(t)$. Let us introduce the parameter α such that $0 \leq \alpha < 1$ and define the function $A(t)$:

$$A(t) = \begin{vmatrix} 1 - \alpha & \text{, if } 0 \leq (t \text{ modulo } 1) < \alpha \\ \cos\left(2\pi\frac{t-\alpha}{1-\alpha}\right) - \alpha & \text{, if } \alpha \leq (t \text{ modulo } 1) < 1 \end{vmatrix} \tag{8}$$

The plot of the amplitude $A(t)$ is displayed Fig. 2. If $\alpha = 0$ is zero, $A(t) = \cos(2\pi t)$ and the problem is symmetric. Otherwise, the pressure difference is constant during the first step in the interval $[t_0, t_0 + \alpha[$ followed by a sinusoidal pumping in the interval $[t_0 + \alpha, t_0 + 1[$. In this case $A(t + 1/2) \neq -A(t)$. Note that the mean value of the pumping is still zero if $\alpha \neq 0$. The advantage of the temporal asymmetry compared to the asymmetric geometry is that the particle direction can be controlled by changing only the pumping.

According to Beltrame et al. (2016), particle transport via the ratchet effect is a generic feature of equations of the same kind as Eq. 6 which have a spatial and temporal periodicity. The velocity contrast c_u defined as the relative variation of u_{eq}:

$$c_u = \frac{max(u_{eq}) - min(u_{eq})}{2\,mean(u_{eq})} \tag{9}$$

is a key parameter as it needs to be large enough for transport to take place. This parameter is related to the camber c_r and the particle radius r_p. In Makhoul et al. (2015a) and Makhoul (2016), we showed that the velocity contrast increases with c_r up to a maximum value of about $c_u \simeq 0.5$. Figure 3a displays the profiles $u_{eq}(x)$ for a pore shape such as $c_r = 0.56$ and $r_{min} = 0.14$ (minimal radius) and for two particle radii $r_p = 0.05$ or $r_p = 0.1$. The particle size does not notably affect the velocity contrast which remains about 0.5. This result is expected since this velocity field $u_{eq}(x)$ corresponds to a kind of a mean effect of the fluid velocity field over the particle domain. In contrast, the friction $\gamma(x)$ is very sensitive to the particle size in a
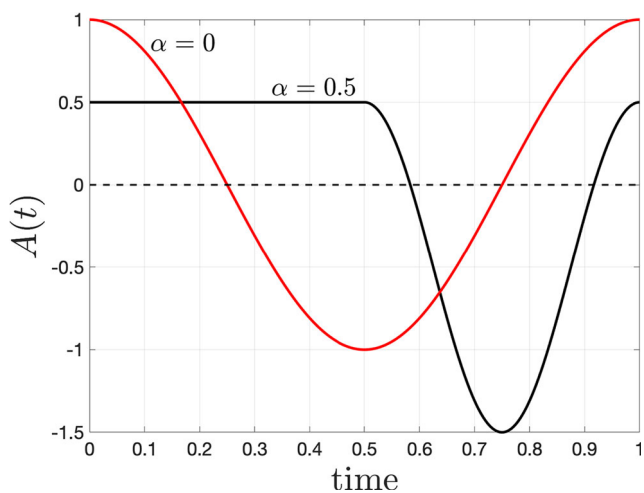
Fig. 2 Time evolution of the pumping amplitude $A(t)$ for $\alpha = 0$ (red sinusoidal curve) and $\alpha = 0.5$ (black curve)

Fig. 4 [Color online] Time evolutions of the periodic solutions s_0, s_m and s_a for $r_p = 0.05, \alpha = 0, \mathcal{P}_\gamma = 79$ and $\mathcal{P}_v = 676$. Other parameters as in Fig. 3. The mean values of s_0 and s_m are 0 and $-1/2$ respectively while the asymmetric s_a has a mean value that is slightly negative: $<s_m> = -0.13$

confined geometry according to (Happel and Bryne 1954). For $r_p = 0.05$ the friction varies slightly while for $r_p = 0.1$, the friction contrast is high (Fig. 3b). The large friction contrast may induce a friction ratchet (Reimann 2002).

In the following, we fix the pore shape to $r_m = 0.315$, $c_r = 0.56$ and we consider two particle sizes: $r_p = 0.05$ or $r_p = 0.1$. We explore the transport dynamics in the parameter space using the time integration and the path-following method of the periodic solutions. The bifurcation parameters are $\mathcal{P}_\gamma, \mathcal{P}_v$ and α. Branches of T-periodic solution on bifurcation diagrams are represented by the norm $||.||$ such that $||s|| = [\frac{1}{T}\int_0^T (\dot{x}(t))^2 dt]^{1/2}$. Thus, the norm does not depend on the particle position.

Transition to Transport

For overdamped particles, i.e. $\mathcal{P}_\gamma = +\infty$, the particle trajectories are oscillations synchronized with the fluid. According to Beltrame et al. (2016), even for a finite value of $\mathcal{P}_\gamma$ but for sufficiently low values of $\mathcal{P}_v$, i.e. the pumping amplitude, there are two kinds of periodic solutions of the particle motion which are centered at the extrema of the velocity field u_{eq} noted s_0 for the maximum and s_m for the minimum. Examples of time evolutions are displayed in Fig. 4. The s_m solution is stable and is an attractor of all dynamics. In this section we analyze the transition from
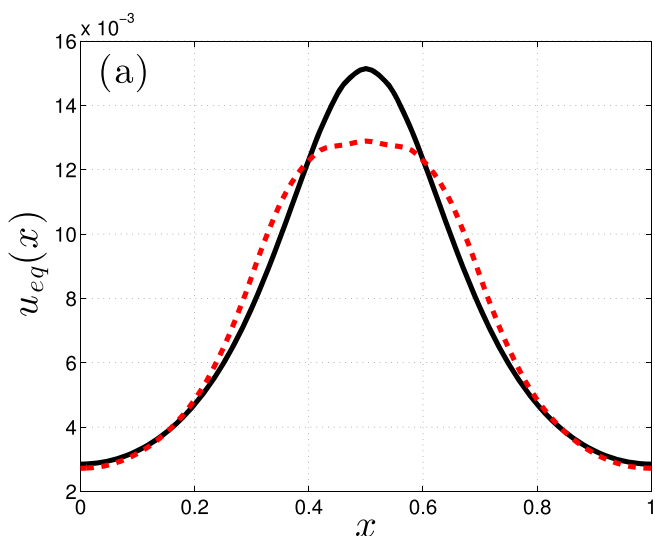
Fig. 3 Profile of (left panel) $u_0(x)$ and (right panel) $\gamma(x)$ functions for two particle radii: (black line) $r_p = 0.05$ and (red dashed line) $r_p = 0.1$. Parameters of the pore shape are $c_r = 0.56$, $r_{min} = 0.14$ and $r_m = 0.315$
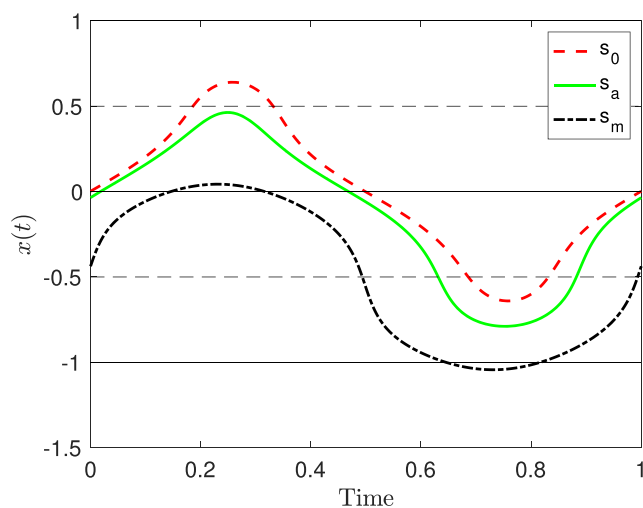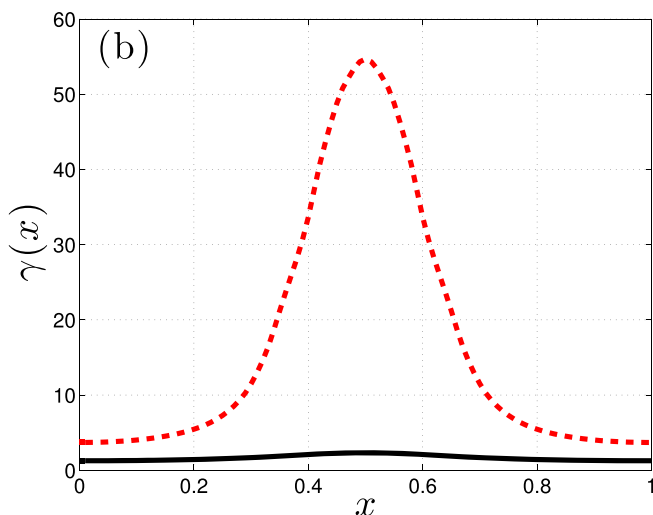
oscillations to transport solutions when the drag $\mathcal{P}_\gamma$ is finite by varying the different parameters.

By the evaluation of the norm $||s||$ of the symmetric solutions s_0 and s_m, we trace the solution branches by increasing $\mathcal{P}_v$ for symmetrical pumping ($\alpha = 0$) and we fix $\mathcal{P}_\gamma$ at 79. The s_0 and s_m solution branches cross regularly, displaying a snakelike structure in the bifurcation diagram (Fig. 5). In the vicinity of the crossing of the branches, the stability of the solutions changes via a supercritical pitchfork bifurcation. From this bifurcation the asymmetric branch s_a, which is stable, emerges and ends (see its time evolution in Fig. 4). Thus, according to Fig. 5 there is a stable and attracting 1-periodic solution for any value of $\mathcal{P}_v$. All the dynamics is attracted by the stable 1-periodic solution and then no transport solution is possible in the symmetric case.

This result is analogous to the model of the point-like particle (Beltrame et al. 2016) for a similar drag. In particular, the transport is possible only via forced symmetry-breaking when the drag $\mathcal{P}_\gamma$ is large. The continuation of periodic branches by varying the α asymmetry of the pumping reveals that the s_0 and s_m branches, and potentially the s_a branch if it exists, end at saddle-node bifurcations. Starting from the s_0 and s_m solutions at $\mathcal{P}_v = 1350$ computed in Fig. 5, the bifurcation diagram (Fig. 6) displays a saddle-node bifurcation at $\alpha_m \simeq 0.2807$ between s_0 and s_m. Note that for these parameters, the s_a branch does not exist. A similar scenario arises

Fig. 6 Continuation of s_0 and s_m periodic solutions for $r_p = 0.05$, $\mathcal{P}_v = 1350$, $\mathcal{P}_\gamma = 79$ by varying α. Plain [dashed] line indicates stable [unstable] orbit. Black dots indicate saddle-node bifurcations at α_m and α_M

starting from $\alpha = 1$ for which the pumping is zero: a pair of saddle orbits annihilate in a saddle-node for $\alpha_M \simeq 0.8143$.

The saddle-node bifurcation corresponds to the intermittent bifurcation type-I (Pomeau and Manneville 1980) as explained in (Beltrame et al. 2016). In the large range [0.3; 0.8], no periodic solution is found. The time evolutions of the particle positions show a drift to negative values of x (Fig. 7). For $\alpha = 0.3$, i.e. near the first saddle-node, we can distinguish two phases of the dynamics. During the first phase the particle oscillates around the same position and after about fifteen oscillations, a slow drift appears during five periods. The representation of the dynamics using the stroboscopic particle position at every time period highlights these two phases. The discrete dynamics resembles a regular descending staircase for different values of α (Fig. 8). The plateaux correspond to oscillations close to the
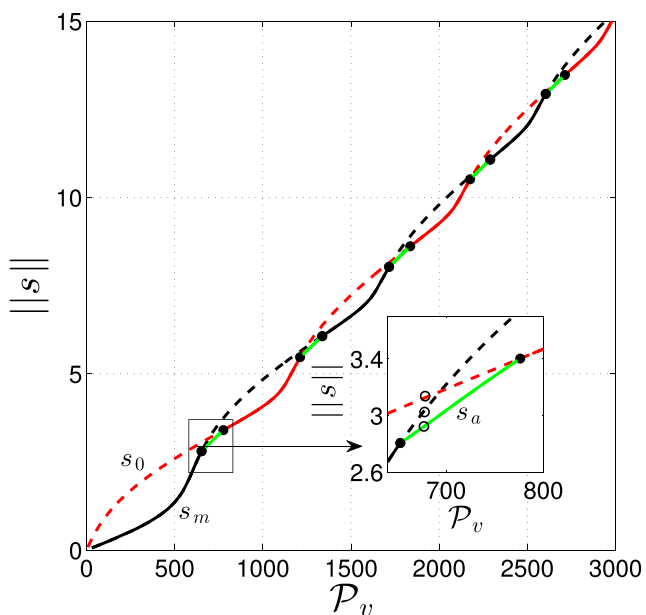

Fig. 5 [Color online] Continuation of 1-periodic solutions of particles for $r_p = 0.05$, $\alpha = 0$ and $\mathcal{P}_\gamma = 79$, by varying $\mathcal{P}_v$. Color code is as follows: (black) s_m, (red) s_0 and (green) s_a. Plain [dashed] line indicates stable [unstable] orbit. Black dots indicate pitchfork bifurcations. Solution profiles indicated by the circle in inset are shown in Fig. 4. Other parameters as in Fig. 3
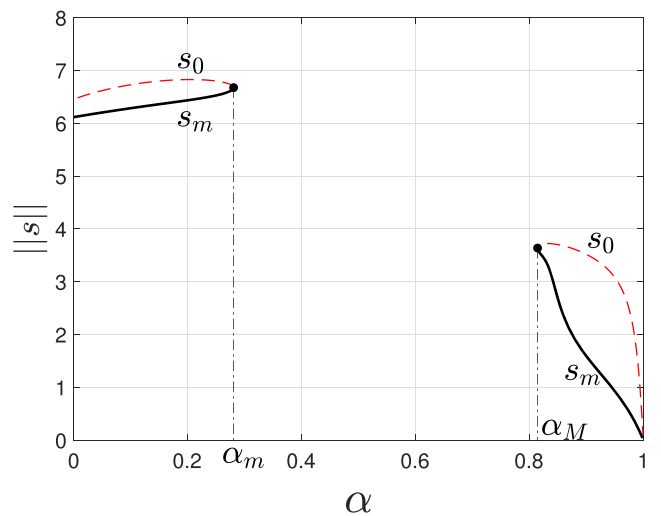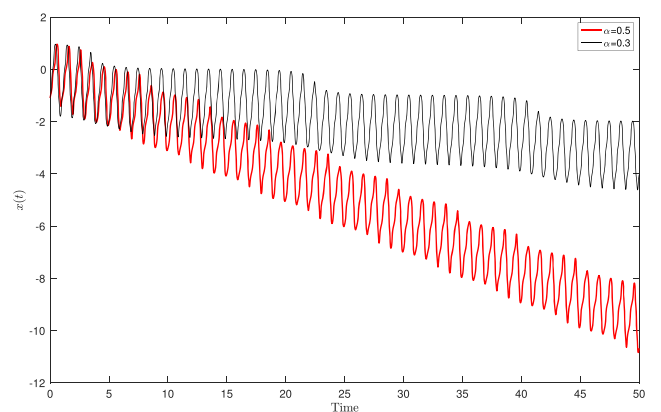

Fig. 7 [Color online] Time evolutions of the particle position $x(t)$ with $r_p = 0.05$ and two values of $\alpha = 0.3$ and 0.5. Other parameters as in Fig. 6
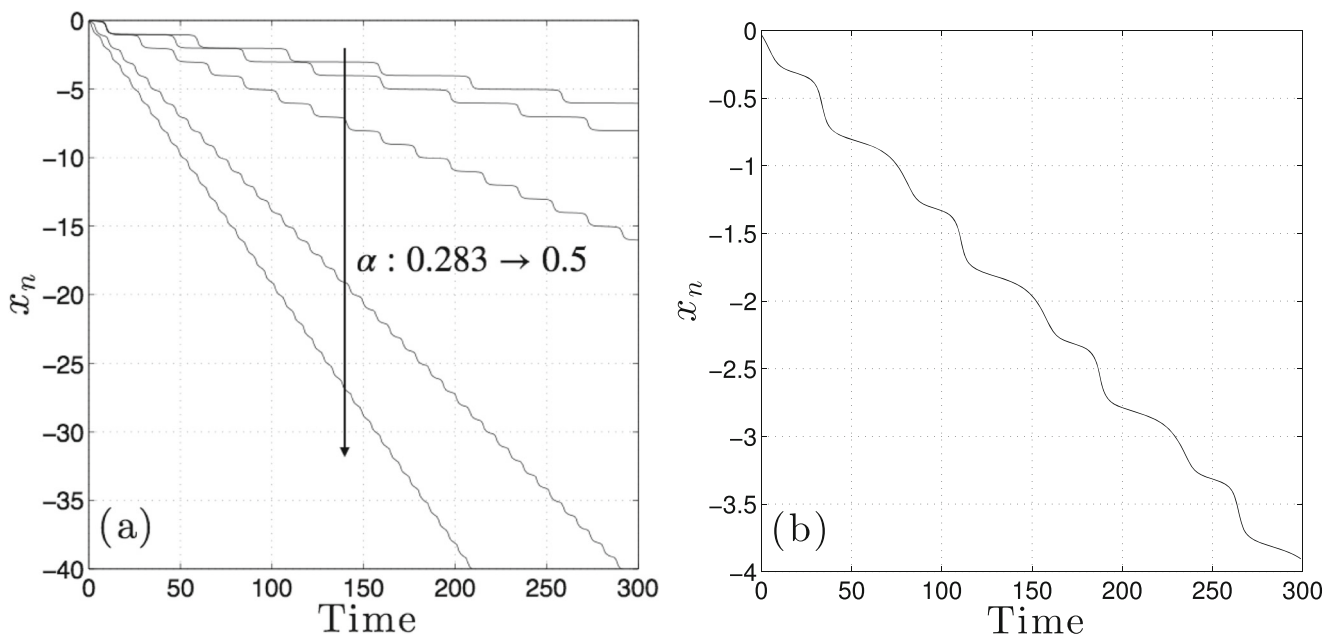
Fig. 8 Discrete particle positions $x_n = x(n)$, $n \in \mathbb{N}$ near the onset. **a** Different values of $\alpha = 0.283; 0.285; 0.3; 0.4; 0.5$, other parameters as in Fig. 6. **b** $\mathcal{P}_v = 1350$, other parameters as in Fig. 9a

threshold. The plateaux become longer when α approaches the onset of bifurcations. Such a dynamics is similar to the phase slip of a desynchronisation transition (Beltrame et al. 2016). A well-known consequence is that the drift velocity vanishes as the square root of the threshold distance: $c \propto \sqrt{\alpha - \alpha_c}$, where α_c is the threshold value.

According to the time integration, the drift velocity increases with α till $\alpha \simeq 0.5$ (see the time evolution in Fig. 7) and remains almost constant till 0.6. By further increasing α the velocity decreases to zero when α approaches the critical value of the second saddle node. Consequently, the optimal transport is about $\alpha = 0.5$. In the next section, we fix α at 0.5 and we seek the parameter domains of particle transport.

Note that according to the discussion in Beltrame et al. (2016), the particle drift phenomenon is part of a class of dissipative rocking ratchets for which the transport direction is determined by the asymmetry (Wickenbrock et al. 2011; Cuesta et al. 2013). In the current problem, it means that the direction of transport depends only on the sign of the α parameter, i.e. the kind of pumping. The particle drifts to negative values of x if $\alpha > 0$, otherwise the particle drifts to positive values.

Domain of Intermittent Drift

We explore the transport domain by varying the parameters $\mathcal{P}_v$ and $\mathcal{P}_\gamma$ and for two radius values, $r_p = 0.05$ and $r_p = 0.1$. The bifurcation diagrams in Fig. 9 show the solution branches s_0 and s_m tracked by varying $\mathcal{P}_v$, all the other

parameters being fixed. The branch ends at a saddle-node for $\mathcal{P}_v$ about 690. In addition, a new pair of saddle-node branches exists in a domain from about 711.7 to 1121. These branches emerge and end at a saddle-node. For larger $\mathcal{P}_v$, a periodic solution branch no longer exists and the time integration displays an intermittent transport solution in the negative direction. Thus, the transport requires pumping with a large amplitude compared to the spatial periodicity. In addition, for $r_p = 0.05$, there is a thin region of transport delimited by the two saddle-nodes of different branches. The time evolution of the particle in Fig. 8b exhibits the influence of both saddle-nodes by displaying two kinds of plateaux. This thin transport region vanishes for $r_p = 0.1$ because the domains of the periodic solutions overlap.

We now trace the saddle-node loci of the periodic solutions, in the $(\mathcal{P}_\gamma, \mathcal{P}_v)$ plane (Fig. 10) which represents the possible onset of transport. By varying $\mathcal{P}_\gamma$ the two saddle-nodes form a vertical band which ends at a minimal value of $\mathcal{P}_\gamma$ except if $\mathcal{P}_v$ is about 1000 (see Fig. 10). The transport arises in the region outside these bands and when the bands do not overlap (gray region in Fig. 10). Therefore, the transport domain is roughly a sector in the $(\mathcal{P}_v, \mathcal{P}_\gamma)$ plane with additional tapered vertical spaces for specific values of $\mathcal{P}_v$ for which transport may occur for large $\mathcal{P}_\gamma$ values. The specific $\mathcal{P}_v$ values are only slightly affected by the particle size: the tapered region occurs for $\mathcal{P}_v$ of about 1500, 2200 and 2900 regardless of r_p. Note that beyond a critical value of $\mathcal{P}_v$ ($\mathcal{P}_\gamma$ is fixed), transport always occurs. The $\mathcal{P}_v$ parameter being proportional to the pressure difference $[p]$, the pumping amplitude and the
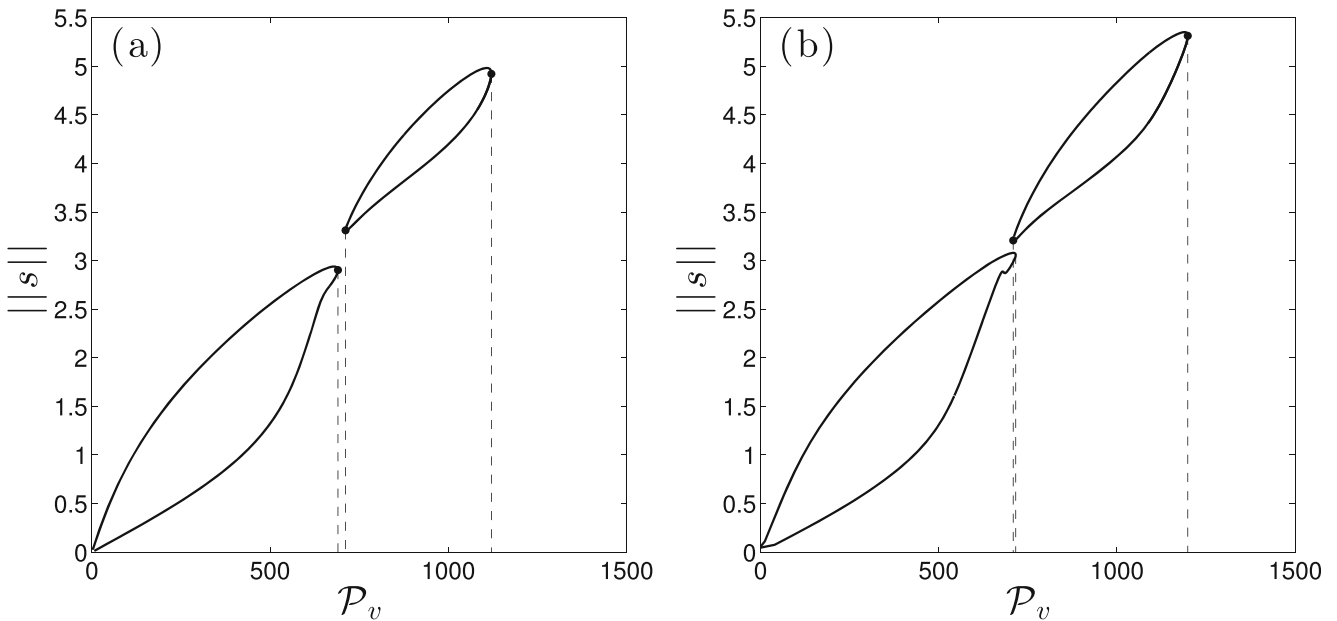
Fig. 9 Continuation of 1-periodic solutions by varying $\mathcal{P}_v$ for **a** $r_p = 0.05$ **b** $r_p = 0.1$. Parameters are $\alpha = 0.5$, $\mathcal{P}_\gamma = 79$

(*Re*) Reynolds number increase. The consistency of the results with the Stokes approximation is analyzed in the next section.

Domain of Validity of the Assumptions

In this section, we analyze the consistency of the parameter domains of the transport with the simplifying assumptions of a quasi-static and isovolume Stokes' flow with no-slip condition described by Eqs. 1 and 2.

First, we discuss the i) isovolume and ii) no-slip assumptions. We show in the following two paragraphs that the error is about a few percent. Then, in the third paragraph iii), we determine the parameter domain for which the quasi-static approximation is valid for an error under 10%.

i) In a general way, the density ρ verifies the dimensional continuity equation

$$\frac{\partial \rho}{\partial t} + \nabla \rho . \vec{v} + \rho \nabla . \vec{v} = 0 \tag{10}$$

We note with a star * the adimensional variables and operators. Lengths, time and velocity are scaled by L, T and V_c, where V_c is the characteristic velocity of the fluid. The pressure variations are scaled by the pressure difference $[p]$ between the outlet and inlet of the pore. Finally, the variations of ρ are scaled by $\delta \rho \simeq \rho_0 \beta [p]$, where β is the compressibility. The air compressibility behaves almost like an ideal gas and so $\beta \simeq 1/p_{atm}$ where p_{atm} is ambient pressure.

Therefore, $\delta \beta \simeq \rho_0 [p]/p_{atm}$ and according to the continuity Eq. 10 :

$$\rho_0 \rho^* \nabla^* . \vec{v}^* \frac{V_c}{L} \propto \frac{\partial \rho^*}{\partial t^*} \rho_0 \frac{[p]}{p_{atm}} \frac{V_c}{L} + \rho_0 \frac{[p]}{p_{atm} T} \nabla^* \rho^* . \vec{v}^* \tag{11a}$$

$$\rho^* \nabla^* . \vec{v}^* \propto \frac{[p]}{p_{atm}} \left(\frac{L}{T V_c} \frac{\partial \rho^*}{\partial t^*} + \nabla^* \rho^* . \vec{v}^* \right) \tag{11b}$$

The ratio $\frac{L}{T V_c}$ is inferior to 1 according to the results of the previous section. For instance in Fig. 7, the amplitude of particle oscillations during one period is at least superior to L and then it is the case of the fluid also. Moreover, since $[p]/p_{atm} \ll 1$ then $\nabla^* . \vec{v}^* \ll 1$ according to Eq. 11b. This justifies the approximation of Eq. 2.

The compressibility also has an influence on the viscosity forces: in addition to $\mu \Delta \vec{v}$, there is a second term: $\lambda \nabla(\nabla . \vec{v})$ due to the bulk viscosity λ. According to the previous scaling, the magnitude of the latter term is $\mu [p]/p_{atm} V_c/L^2$ while the magnitude of the first term is $\mu V_c/L^2$. Then the ratio between the second additional term and the first one is $[p]/p_{atm} \ll 1$, in other words it is negligible.

ii) For a gas flow in a microchannel, one expects a slip velocity v_s at the boundary such that Colin (2005) and Qin et al. (2007):

$$v_s = b \left. \frac{\partial v}{\partial r} \right|_{\text{channel boundary}} \tag{12}$$

where b is the slip length. The slip velocity is of the same order of magnitude as the mean free path λ (Maali et al. 2016). For air, $\lambda = 65 nm$ in standard
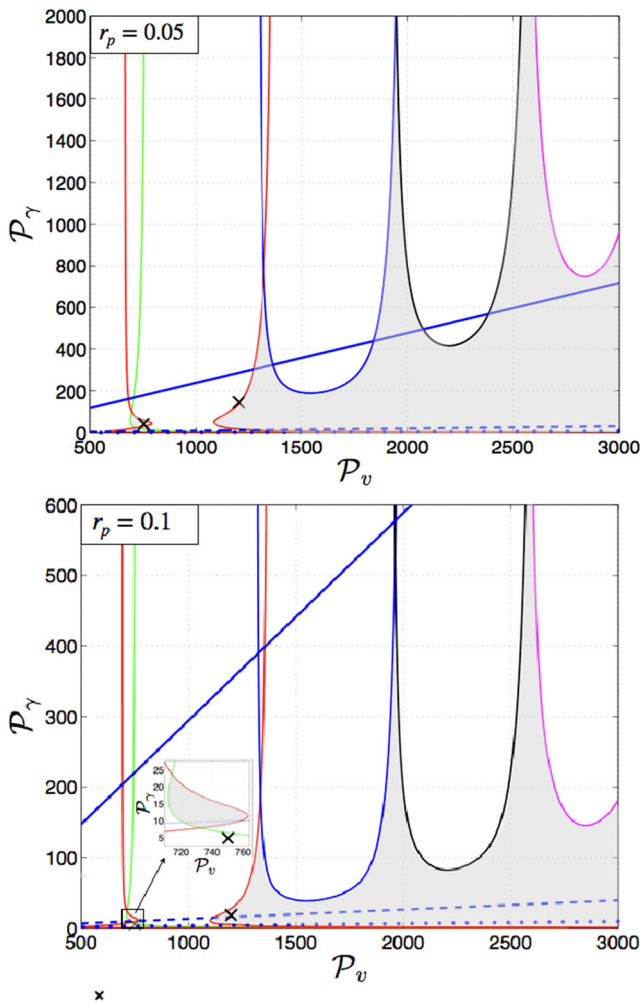
Fig. 10 [Color online] Saddle-node loci of 1-periodic solutions in the $(\mathcal{P}_\gamma, \mathcal{P}_v)$ plane for the particle sizes $r_p = 0.05$ and 0.1. The gray region displays the domain of intermittent drift. The lines display the lower limit of the validity of the Stokes approximation for different density ratios between particles and fluid. The × symbols correspond to the values of the examples of the Section "Domain of Validity of the Assumptions". Other parameters are as in Fig. 9

conditions of pressure and temperature (Colin 2005). Approximating the shear $\frac{\partial v}{\partial r}$ by V_c/R_m, the slip velocity is about

$$v_s \simeq K_n V_c, \tag{13}$$

where $K_n = \frac{\lambda}{R_m}$ is the Knudsen number. Assuming $L = 10\mu m$ (see paragraph iii)), then $R_m = L r_m \simeq 3\mu m$. Finally $K_n \simeq 2 \cdot 10^{-2}$. Then, according to (13) the slip velocity v_s is about a few percent of the characteristic velocity V_c.

Therefore, assuming a no-slip boundary implies an error of a few percent on the fluid velocity field. Because the resulting drag force R_x depends linearly on the velocity field, the relative error made on R_x is similar to the relative error of the velocity field.

iii) The Stokes approximation Eq. 1 is valid if the convective acceleration and the local acceleration are small compared to the viscous dissipation. These approximations are questionable since the existence of transport is related to a minimal value of $\mathcal{P}_v$. As the latter is proportional to the pressure difference $[p]$, the (Re) Reynolds number may be large in the transport domains shown in Fig. 10. In the following, we determine the sub-domains for which Re is small.

The convective acceleration is scaled by Re while for an oscillating flow of period T the local acceleration is scaled by the number noted Re_{loc} which is the product of the Reynolds and the (St) Strouhal numbers. Using the same scaling as previously, the dimensionless numbers read $Re = \frac{\rho_0 V_c L}{\mu}$ and $Re_{loc} = Re St = \frac{\rho_0 L^2}{\mu T}$. We approximate the characteristic fluid velocity V_c with the mean velocity of the Poiseuille flow in a cylindrical tube with the mean radius r_m under the pressure gradient $[p]/L$, which gives $V_c \simeq \frac{r_m^2 L [p]}{8\mu}$. Then, the $\mathcal{P}_v$ and $\mathcal{P}_\gamma$ numbers are related to the Re and Re_{loc} numbers by:

$$Re = \frac{3}{32\pi} \frac{\rho_0}{\rho_p} \frac{r_m^2}{r_p^3} \frac{\mathcal{P}_v}{\mathcal{P}_\gamma} \tag{14}$$

$$Re_{loc} = \frac{3}{4\pi} \frac{\rho_0}{\rho_p} \frac{1}{r_p^3} \frac{1}{\mathcal{P}_\gamma} \tag{15}$$

The flow is quasi-static if Re and Re_{loc} are smaller than a small number ϵ which leads to the following conditions:

$$\mathcal{P}_\gamma > \frac{K_1}{\epsilon} \mathcal{P}_v \quad \text{with } K_1 = \frac{3}{32\pi} \frac{\rho_0}{\rho_p} \frac{r_m^2}{r_p^3} \tag{16a}$$

$$\mathcal{P}_\gamma > \frac{K_2}{\epsilon} \quad\quad \text{with } K_2 = \frac{3}{4\pi} \frac{\rho_0}{\rho_p} \frac{1}{r_p^3} \tag{16b}$$

The condition Eq. 16b is verified as long as Eq. 16a is verified and $\mathcal{P}_v$ is superior to $8/r_m^2 \simeq 80$ for $r_m = 0.315$. As the studied transport solutions studied here occur for $\mathcal{P}_v > 500$, we consider only the condition Eq. 16a in the following. The latter condition defines a line with a positive slope: the validity range of the quasi-static approximation lies in the upper half plane of the line. In Fig. 10 (intermittent drift) we have drawn this limit for $\epsilon = 0.1$ and the density ratios ρ_p/ρ_0 equal to [plain line] 100, [dashed line] 2,250 and [dotted line] 9,460. According to the diagrams in Fig. 10, the density ratio has to be approximately greater than 100 for $r_p = 0.05$ and greater than 1000 for $r_p = 0.1$. Such large ratios between the fluid and the particle are possible for a gas and a solid particle such as air and a metal particle. For instance the ratios 2,250 and 9,460 plotted in Fig. 10 correspond respectively to the density ratios of air/aluminum and air/lead.

In the parameter range of the Stokes approximation, it is possible to obtain a selective transport depending on the particle radius. For instance, if $\mathcal{P}_v = 1200$ and $\mathcal{P}_\gamma = 18.0$ for $r_p = 0.1$, there is an intermittent drift with $c = -0.18$ (see Fig. 10). In contrast, if $r_p = 0.05$ and if all other physical parameters remain then $\mathcal{P}_v = 1200$, $\mathcal{P}_\gamma = 144$ and according to Fig. 10 no transport occurs. These parameters can be realized by considering an aluminum particle in microgravity in air at ambient temperature and pressure. Let us consider a channel with $L = 10\mu m$ periodicity and $T = 1.1ms$ periodic pumping and spherical particles with $R_p = 0.5\mu m$ or $1\mu m$. The amplitude of pressure pumping between the inlet and outlet of the pore is $[p] = 20Pa$. In this case, transport occurs with the drift velocity $c_{dim} = -1.6mm/s$ for the larger particle ($R_p = 1\mu m$) and no transport for $R_p = 0.5\mu m$.

By considering larger density particles such as lead, the selectivity of the transport can be reversed. For instance, with the physical parameters $L = 10\mu m$, $T = 1.3ms$, $[p] = 11Pa$ and lead particles with $R_p = 1\mu m$ or $R_p = 0.5\mu m$, only the smaller particles ($R_p = 0.5\mu m$) drift with $c_{dim} = -0.55mm/s$. In Fig. 10, these parameters correspond to the leftmost $\times$ in the existence domains: for $r_p = 0.05$, $(\mathcal{P}_v, \mathcal{P}_\gamma) = (750, 40)$ is located in a small 'island' of the transport domain whereas for $r_p = 0.1$ the point $(\mathcal{P}_v, \mathcal{P}_\gamma) = (750, 5)$ is outside the transport domain (see $\times$ symbol in the inset of Fig. 10).

In each of these examples, the particles need less than 2 seconds to pass through a 1mm thick membrane separating two basins. This is suitable for short duration microgravity experiments such as in a zero-g flight or in a drop tower. The advantage of the latter is that the noise due to g-jitter is lower.

Concluding Remarks

Using time-integration and bifurcation analysis, we have shown that the transport of micro-particles is possible under an oscillating Stokes flow and that it differs from the stochastic drift ratchet (Kettner et al. 2000). The transport occurs via desynchronization of the trivial periodic solutions as mentioned in Beltrame et al. (2016) for the ratchet model with point-like particles. Such a mechanism could be applied to the selective transport of micro-particles of metal in suspension in air under a micro-gravity environment. With a pore size of about ten microns and a fluid such as air and metal particles, it would be possible to observe this selective transport during the short duration of micro-gravity experiments such as in a drop tower or in a zero-g flight. The author of Beltrame (2018) showed that noise triggers the transport for specific parameters in ratchet systems. Therefore, particle transport could still be effective even in the presence of g-jitter.

Our analysis is based on a simple model. More accurate computation can be performed by taking into account the slip boundary condition. Moreover, many questions are still open regarding the stability of the particle trajectory along the axis and also the interaction between particles. However the resulting additional non-linear mechanisms do not forbid the existence of a ratchet effect. Indeed, transport phenomena are mainly due to space and time periodicities and field contrast.

Finally, there is another transport mechanism for heavy particles such as lead that corresponds to a synchronized transport described in Beltrame et al. (2016). The dynamics are more complex than those described here. In particular, the direction of transport does not only depend on the sign of α. Their domain of existence lies essentially in the region of the parameters where the Reynolds number is not negligible. Taking into account the inertia of fluids would be a much more difficult task because the motion of particles is no longer governed by an ODE system but by the Navier-Stokes EDP. Such a study is the subject of a future project.

References

Beltrame, P.: Absolute negative mobility in ratchets: Symmetry, chaos and noise. J. Chaotic Model. Simul. **1**, 101–114 (2018)

Beltrame, P., Makhoul, M., Joelson, M.: Deterministic particle transport in a ratchet flow. Phys. Rev. E **93**, 012208 (2016)

Brenner, H.: Effect of finite boundaries on the stokes resistance of an arbitrary particle part 2. asymmetrical orientations. J. Fluid Mech. **18**, 144–158 (1964)

Cherepanov, I.N., Smorodin, B.L.: Convective flow of a colloidal suspension in a vertical slot heated from side wall. Microgravity Sci. Technol. **30**, 63–68 (2018)

Colin, S.: Rarefaction and compressibility effects on steady and transient gas flows in microchannels. Microfluid Nanofluid **1**, 268–279 (2005)

Cuesta, J.A., Quintero, N.R., Alvarez-Nodarse, R.: Time-shift invariance determines the functional shape of the current in dissipative rocking ratchets., vol. 3. https://doi.org/10.1103/PhysRevX.3.041014 (2013)

Hänggi, P., Marchesoni, F.: Artificial brownian motors: Controlling transport on the nanoscale. Rev. Mod. Phys. **81**, 387–442 (2009)

Happel, J., Bryne, B.: Motion of a sphere in a cylindrical tube. Ind. Eng. Chem. **56**(6), 1181–1186 (1954)

Kettner, C., Reimann, P., Hänggi, P., Müller, F.: Drift ratchet. Phys. Rev. E **61**(1), 312–323 (2000)

Kulrattanarak, T., van der Sman, R., Schroënn, C., Boom, R.: Classification and evaluation of microfluidic devices for continuous suspension fractionation. Adv. Colloid Interface Sci. **142**(1), 53–66 (2008)

Loutherback, K., Puchalla, J., Austin, R.H., Sturm, J.C.: Deterministic microfluidic ratchet. Phys. Rev. Lett. **102**, 045301 (2009)

Luchsinger, R.H.: Transport in nonequilibrium systems with position-dependent mobility. Rev. Phys. E **62**, 272–275 (2000)

Maali, A., Colin, S., Bhushan, B.: Slip length measurement of gas flow, vol. 27 (2016)

Makhoul, M.: Modélisation du transport de particule dans un écoulement de stokes á effet cliquet. Ph.D. thesis, Université d'Avignon (2016)

Makhoul, M., Beltrame, P., Joelson, M.: Drag force on a confined particle: Particle transport. Int J Mech **9**, 260 (2015)

Makhoul, M., Beltrame, P., Joelson, M.: Particle drag force in a periodic channel: wall effects. In: Topical Problems of Fluid Mechanics : Proceedings. Prague, pp 141–148 (2015)

Mathwig, K., Müller, F., Gösele, U.: Particle transport in asymmetrically modulated pores. New J. Phys. **13**(3), 033038 (2011)

Matthias, S., Müller, F.: Asymmetric pores in a silicon membrane acting as massively parallel brownian ratchets. Nature **424**, 53–57 (2003)

Pomeau, Y., Manneville, P.: Intermittent transition to turbulence in dissipative dynamical systems. Commun. Math. Phys. **74**, 189–197 (1980)

Qin, F.H., Sun, D.J., Yin, X.Y.: Perturbation analysis on gas flow in a straight microchannel. Phys. Fluids **19**, 027103 (2007)

Reimann, P.: Brownian motors: noisy transport far from equilibrium. Phys. Rep. **361**, 57–265 (2002)

Santamaria, F., Boffetta, G., Afonso, M.M., Mazzino, A., Onorato, M., Pugliese, D.: Stokes drift for inertial particles transported by water waves. EPL (Europhysics Letters) **102**(1), 14003 (2013)

Vlasova, O., Karpunin, I., Latyshev, D., Kozlov, V.: Steady flows of a fluid oscillating in an axisymmetric channel of variable cross-section, versus the dimensionless frequency. Microgravity Sci. Technol. **32**(3), 363–368 (2020)

Wickenbrock, A., Cubero, D., Wahab, N.A.A., Phoonthong, P., Renzoni, F.: Current reversals in a rocking ratchet: The frequency domain. Phys. Rev. E **84**, 021127 (2011)